Mitochondrial Function in Diabetes: Novel Methodology and New Insight

Liping Yu,[1] Brian D. Fink,[2] Judith A. Herlein,[2] and William I. Sivitz[2]

Interpreting mitochondrial function as affected by comparative physiologic conditions is confounding because individual functional parameters are interdependent. Here, we studied muscle mitochondrial function in insulin-deficient diabetes using a novel, highly sensitive, and specific method to quantify ATP production simultaneously with reactive oxygen species (ROS) at clamped levels of inner mitochondrial membrane potential ($\Delta\Psi$), enabling more detailed study. We used a 2-deoxyglucose (2DOG) energy clamp to set $\Delta\Psi$ at fixed levels and to quantify ATP production as 2DOG conversion to 2DOG-phosphate measured by one-dimensional ^{1}H and two-dimensional $^{1}H/^{13}C$ heteronuclear single quantum coherence nuclear magnetic resonance spectroscopy. These techniques proved far more sensitive than conventional ^{31}P nuclear magnetic resonance and allowed high-throughput study of small mitochondrial isolates. Over conditions ranging from state 4 to state 3 respiration, ATP production was lower and ROS per unit of ATP generated was greater in mitochondria isolated from diabetic muscle. Moreover, ROS began to increase at a lower threshold for inner membrane potential in diabetic mitochondria. Further, ATP production in diabetic mitochondria is limited not only by respiration but also by limited capacity to use $\Delta\Psi$ for ATP synthesis. In summary, we describe novel methodology for measuring ATP and provide new mechanistic insight into the dysregulation of ATP production and ROS in mitochondria of insulin-deficient rodents. ***Diabetes*** **62:1833–1842, 2013**

According to the widely accepted chemiosmotic theory, oxidative phosphorylation uses the electrochemical gradient across the inner mitochondrial membrane ($\Delta\Psi$) to drive ATP production (1). In this process, protons move inward with the charge gradient, driving the rotary component of ATP synthase in stepwise fashion to bind ADP, phosphorylate ADP, and release ATP to the matrix (2,3). Oxidative phosphorylation has been divided into three modules that independently control $\Delta\Psi$ (4). Each act in different fashions to either supply or consume $\Delta\Psi$ (Fig. 1). These modules include supply by respiration, consumption by proton leaks, and consumption for ATP synthesis.

Major metrics used to describe mitochondrial function include oxygen consumption (respiration), membrane potential, the rate of ATP production, and generation of reactive oxygen species (ROS) in the form of superoxide. Respiration as measured in isolated mitochondria is proportional to electron transport. In recent work (5), we underscored the importance of considering mitochondrial ROS production not only as an isolated entity but also in relation to electron transport, the process from which electron leaks derive. We showed that absolute ROS production by muscle mitochondria of insulin-deficient rats was reduced, but it was substantially increased when viewed as a function of respiration (electron transport).

In this study, we further investigated the relationships between parameters of muscle mitochondrial function as affected by insulin deficiency. In particular, we examined ATP production in a way that provides new information about contributions of the modular components (Fig. 1) to the process. We also examined ROS production as affected at different levels of ATP production as respiration proceeds from state 4 to state 3.

To achieve our objectives, we developed a novel, highly sensitive, and specific ATP assay that can be performed with high throughput in samples obtained from small-volume mitochondrial isolates. ROS production can be assayed simultaneously. The purpose of this report is two-fold, to describe this assay and to provide new insight into mitochondrial function as affected by insulin-deficient diabetes.

RESEARCH DESIGN AND METHODS

Materials. Reagents were purchased as indicated or were from standard sources.

Animal studies. Male Sprague-Dawley rats were obtained from Harlan (Indianapolis, IN). Animals were fed standard chow (Harlan Tekland #7001) and maintained according to National Institutes of Health guidelines. The protocol was approved by our institutional Animal Care Committee. Rats were killed by incision of the left ventricle after injection of 100 mg/kg i.p. pentobarbital, a dose that does not affect mitochondrial respiration or potential (6).

Rats were made diabetic with intraperitoneal streptozotocin (STZ) 60 mg/kg. Controls received vehicle (saline). Rats were killed at ~1000 h, 2 h after removal of food. Gastrocnemius muscle was removed, washed, blotted, and weighed before preparation of mitochondria. Two animal protocols were followed (Fig. 2). Each included three groups of animals: STZ diabetic (STZ-DM), STZ diabetic treated with insulin (DM-INS), and controls (injected with saline as vehicle for STZ). Ages at onset of protocols 1 and 2 were 110 ± 0 and 98 ± 1 days, respectively, with no differences between groups within each protocol. Weight differentials between control and STZ-DM rats (an indicator of severity of diabetes) were similar for protocols 1 and 2. The duration of insulin treatment in protocol 2 was less by intent. Protocol 1 was performed to assess ATP and ROS production and their relationship with clamped membrane potential. Protocol 2 was performed to assess the effect of insulin-deficient diabetes on the capacity to use membrane potential (module 3 of Fig. 1). However, we included some short-duration insulin-treated diabetic rats in protocol 2, mainly to determine if this was sufficient to improve defective ATP production. Insulin-treated rats of protocol 1 received 4 units s.c. glargine insulin daily at 1600–1700 h. Insulin-treated rats of protocol 2 received 6 units s.c. of glargine insulin daily at 1600–1700 h. Although the rats of protocol 1 regained weight, glucose was not well-controlled, prompting the higher dose in protocol 2. Tail-vein glucose at euthanization was >500 mg/100 mL (values >600 were beyond the range of the glucose meter) in all STZ-DM rats as well as in the DM-INS rats in both protocols despite insulin therapy and weight gain (Fig. 2).

From the [1]NMR Core Facility and Department of Biochemistry, University of Iowa, Iowa City, Iowa; and the [2]Department of Internal Medicine and Endocrinology, University of Iowa and the Iowa City Veterans Affairs Medical Center, Iowa City, Iowa.
Corresponding author: William I. Sivitz, william-sivitz@uiowa.edu.
Received 23 August 2012 and accepted 3 December 2012.
DOI: 10.2337/db12-1152
This article contains Supplementary Data online at http://diabetes.diabetesjournals.org/lookup/suppl/doi:10.2337/db12-1152/-/DC1.

See accompanying commentary, p. 1826.

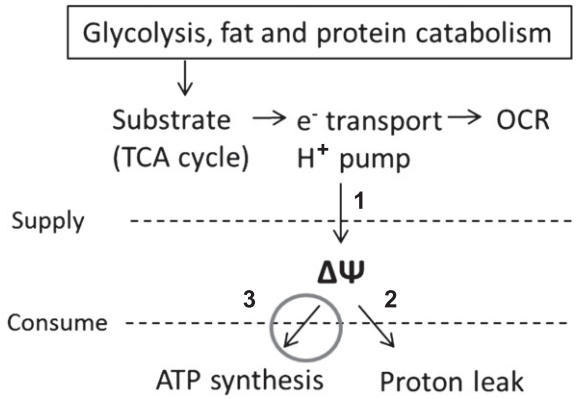

FIG. 1. Modular components regulating oxidative phosphorylation. Module 1 generates the charge gradient (ΔΨ) through proton pumping at respiratory complexes I, III, and IV. Module 2 consumes ΔΨ through proton leak pathways including catalysis through uncoupling proteins, action of the mitochondrial permeability transition pore, or other specific or nonspecific processes. Module 3 (circle) consumes ΔΨ for ATP synthesis. TCA, tricarboxylic acid; OCR, oxygen consumption rate.

Isolation of mitochondria. Muscle mitochondria were isolated as previously described (7–9). Mitochondrial protein was determined on homogenates by the Bradford technique using a kit from Bio-Rad (Hercules, CA). Mitochondria prepared in this fashion were highly pure, as indicated by the distribution of glyceraldehyde-3-phosphate dehydrogenase and porin in whole tissue and mitochondrial extracts (8). Mitochondrial integrity was assessed by cytochrome C release (Cytochrome c Oxidase Assay Kit; Sigma-Aldrich) in several preparations (seven each) for control, diabetic, and insulin-treated diabetic mitochondria. Values for intact mitochondria were 94.4 ± 4.8, 98.3 ± 2.4, and 94.3 ± 3.8%, respectively, which were well within an acceptable range compared with mitochondrial preparations from several sources (10).

Respiration and potential. Respiration and ΔΨ were determined as we previously described (11,12) using a 600-μL respiratory chamber fitted with a tetraphenylphosphonium electrode. Mitochondria (0.5 mg/mL) were incubated in ionic respiratory buffer (120 mmol/L KCl, 5 mmol/L KH_2PO_4, 2 mmol/L $MgCl_2$, 1 mmol/L EGTA, 3 mmol/L HEPES [pH 7.2] with 0.3% fatty acid–free BSA).

Mitochondrial ROS production by fluorescent measurement. H_2O_2 production was assessed using the fluorescent probe 10-acetyl-3,7-dihydroxyphenoxazine (DHPA or Amplex Red; Invitrogen), a highly sensitive and stable substrate for horseradish peroxidase and a well-established probe for isolated mitochondria (13). Fluorescence was measured and quantification was performed as previously described (12). Addition of catalase, 500 units/mL, reduced fluorescence to below the detectable limit, indicating specificity for H_2O_2. Addition of substrates to respiratory buffer without mitochondria did not affect fluorescence.

2-Deoxyglucose as an ATP energy clamp. To assess mitochondrial functional parameters at fixed ΔΨ, we used excess 2-deoxyglucose (2DOG) (5 mmol/L) and hexokinase (HK; 5 units/mL) to generate an "ATP energy clamp" (Fig. 3*A*). The conversion of 2DOG to 2DOG phosphate (2DOGP) occurs rapidly and irreversibly, thereby effectively clamping ADP concentrations and ΔΨ dependent on the amount of exogenous ADP added. This enables titration of membrane potential at different fixed values, whereas mitochondria transit from state 4 (no ADP, maximal potential) to state 3 (high levels of ADP resulting in reduced ΔΨ). The 2DOG clamp has been used in the past to assess mitochondrial-bound hexokinase activity at constant ADP (14), but not to assess mitochondrial physiology or ATP production as described herein.

Use of the 2DOG ATP energy clamp to quantify ATP production in isolated mitochondria and simultaneous assessment of H_2O_2 production. Mitochondria (0.1 mg/mL) were added to individual wells of 96-well plates in a total volume of 60 μL and incubated at 37°C in respiratory buffer plus 5 units/mL HK (Worthington Biochemical) and 5 mmol/L 2DOG or, in some experiments, [6-^{13}C]2DOG (Cambridge Isotope Laboratories, Andover MA) in the presence of ADP or ATP ranging from 0 to 1,000 μmol/L, depending on the particular experiment. After incubation for the desired time, the contents of the microplate wells were removed to tubes on ice containing 1 μL of 120 μmol/L oligomycin to inhibit ATP synthase. Tubes were then centrifuged 4 min at 14,000*g* to pellet the mitochondria. Supernatants were transferred to new tubes and held at −20°C until nuclear magnetic resonance (NMR) analysis. To prepare the NMR sample, 40 μL assay supernatant was added to a 5-mm (outer diameter) standard NMR tube (Norell) along with 50 μL deuterium oxide (D_2O) and 390 μL buffer consisting of 120 mmol/L KCl, 5 mmol/L KH_2PO_4, and 2 mmol/L $MgCl_2$ (pH 7.2).

ATP production rates were calculated based on the percent conversion of 2DOG to 2DOGP, the initial 2DOG concentration, incubation volume, and incubation time. To simultaneously assess H_2O_2 production, mitochondrial incubations were performed in the presence of DHPA as described.

NMR spectroscopy. NMR spectra were collected at 37°C on a Bruker Avance II 500 NMR spectrometer. The 2DOG and 2DOGP ^{1}H and ^{13}C NMR resonances were assigned through ^{1}H homonuclear two-dimensional DQF-COSY (15) and TOCSY (16,17) experiments and ^{1}H/^{13}C two-dimensional heteronuclear

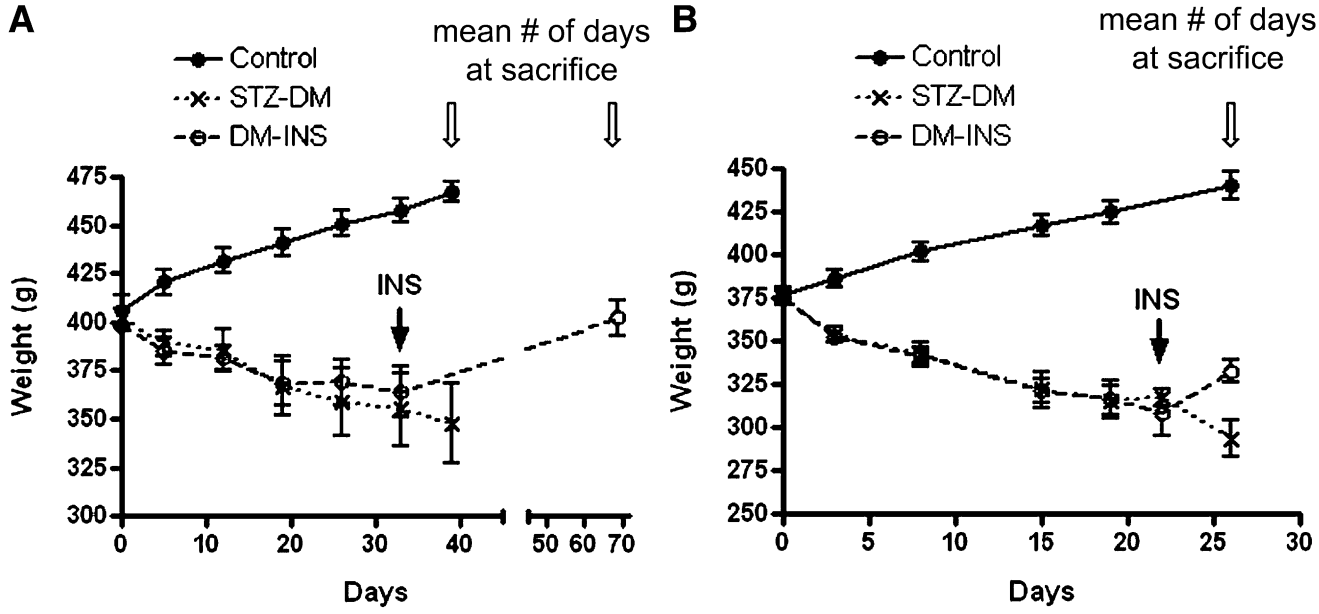

FIG. 2. Weight change (mean ± SE) after injection of STZ 60 mg/kg or vehicle (saline) on day 0 in control, STZ-DM, or DM-INS rats. Diabetes was diagnosed based on a glucose >300 mg/100 mL within 5 days of STZ. Lantus insulin (INS) was administered to the DM-INS rats daily starting at the day number indicated by the *arrow*. The last time points indicated (*open arrows*) represent the average day number at euthanization. *A*: Protocol 1. Rats were killed after the average number of days indicated (range, 34–43 days for control and STZ-DM; 66–68 for DM-INS; *n* = 8, 8, and 7 for control, STZ-DM, and DM-INS groups). *B*: Protocol 2. Rats were killed after the average number of days indicated (range, 21–35 days for all groups; *n* = 8, 7, and 7 for control, STZ-DM, and DM-INS groups).

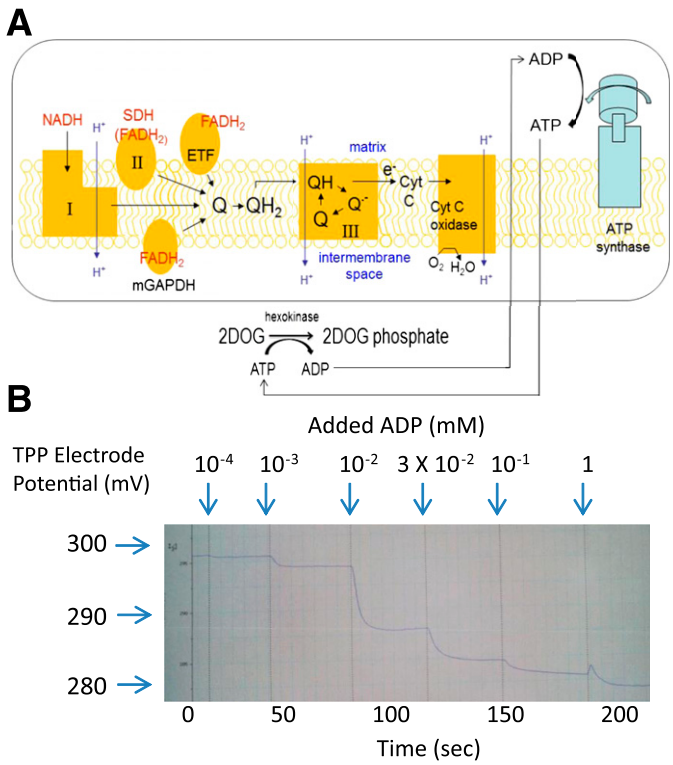

FIG. 3. The 2DOG energy clamp. *A*: Saturating amounts of 2DOG and hexokinase recycle ATP back to ADP by irreversibly converting 2DOG into 2DOGP. The resulting ADP availability is clamped at levels determined by the amount of ADP added. Complex numbers are indicated in Roman numerals. *B*: Representative tracing of inner membrane potential vs. time obtained by incubating normal rat gastrocnemius mitochondria (0.25 mg/mL) fueled by combined substrates including 5 mmol/L succinate plus 5 mmol/L glutamate plus 1 mmol/L malate. ADP was added in incremental amounts to generate the final total recycling nucleotide phosphate concentrations indicated. After each addition, a plateau potential was reached, consistent with recycling at a steady ADP concentration and generation of a stepwise transition from state 4 to state 3 respiration. Note that the potential shown on the *y*-axis represents negative values of electrode potential (not mitochondrial potential). The actual ΔΨ follows a similar pattern after calculation using the Nernst equation based on the distribution of tetraphenylphosphonium (TPP), external and internal, to mitochondria. ETF, electron transport flavoprotein; Cyt C, cytochrome C.

multiple quantum coherence and heteronuclear multiple bond coherence experiments (18). Mitochondrial samples were studied by NMR spectroscopy by acquiring one-dimensional ^{1}H NMR spectra using unlabeled 2DOG or two-dimensional ^{1}H/^{13}C heteronuclear single quantum coherence (HSQC) NMR spectra (19) using ^{13}C-labeled 2DOG at C6-position, i.e., [6-^{13}C]2DOG, in NMR buffer containing 120 mmol/L KCl, 5 mmol/L KH_2PO_4, 2 mmol/L $MgCl_2$ (pH 7.2), and 90% H_2O/10% D_2O. The amounts of 2DOG and 2DOGP present in the NMR samples were quantitatively measured using the peak intensities of the assigned resonances of these compounds. The ^{1}H and ^{31}P chemical shifts are referenced to 2,2-dimethyl-2-silapentane-5-sulfonate and external 2% H_3PO_4 in D_2O (20), respectively. NMR spectra were processed with the NMRPipe package (21) and analyzed using NMRView software (22).

Other biochemical assays. Glucose was determined on tail-vein blood using a reagent strip and meter (OneTouch Ultra).

Statistics. Data were analyzed by ANOVA, linear regression, or second-order polynomial curve fitting as indicated in the figures or text. Rates of ATP and H_2O_2 production and respiration (±SE) are expressed per milligram of mitochondrial protein.

RESULTS

Effectiveness of the 2DOG ATP energy clamp. For this technique to work as predicted, sequential increases in ADP added to isolated mitochondria should reduce ΔΨ in stepwise fashion. Figure 3*B* shows that with each addition of ADP, ΔΨ rapidly decreased to plateau levels. Adding ATP instead of ADP resulted in nearly identical data, which was as expected given the recycling effect of the clamp. Oxygen consumption increased as expected with each addition of ADP (data not shown) as respiration shifted toward state 3. When this experiment was performed with ATP but in the absence of HK, respiration did not increase and ΔΨ did not decline, consistent with the lack of recycling to ADP.

Validation of coupling of conversion of 2DOG to 2DOGP for quantification of ATP production. To determine whether HK-mediated conversion of 2DOG to 2DOGP reflects ATP production, we examined the ^{31}P NMR spectrum of 0.85 mmol/L ATP dissolved in a buffer containing 5 mmol/L KH_2PO_4, 120 mmol/L KCl, 2 mmol/L $MgCl_2$, and 4.5 mmol/L 2DOG (pH 7.2) plus 10% D_2O in the absence or presence of HK. In the absence of HK, the ^{31}P NMR spectrum obtained, as expected, was composed of three peaks (α, β, γ) from ATP and one peak (Pi) from the buffer phosphate (Supplementary Fig. 1*A*). However, on addition of HK (5 units/mL), the ATP fully converted to ADP with concurrent formation of 2DOGP from 2DOG (Supplementary Fig. 1*B*). The Pi peak of the sample with HK present is shifted slightly toward right because of the slightly increased acidity (pH, 7.05) of the sample as a result of ATP hydrolysis during the conversion of 2DOG into 2DOGP.

Comparison of ^{1}H and ^{31}P NMR sensitivity. Traditionally, ATP production has been measured directly through detection of the ATP signals via ^{31}P NMR spectroscopy in which the three phosphate signals α, β, γ (Supplementary Fig. 1*A*) are well-resolved from each other and from other ^{31}P signals. However, because of the much smaller magnetogyric ratio of ^{31}P than ^{1}H nuclei, ^{31}P NMR is inherently much less sensitive than ^{1}H NMR. Moreover, the NMR probes routinely accessible in many NMR laboratories, including the triple resonance probe and broadband observe probe, provide significantly superior ^{1}H than ^{31}P signal sensitivity. As shown in Supplementary Fig. 2, for the samples prepared at the same concentration and the data collected with identical acquisition time, the ^{1}H NMR spectrum of 2DOGP provides a much improved signal-to-noise ratio, e.g., 580 for the 2α′ proton (Supplementary Fig. 2*A*), than the ^{31}P NMR spectrum of ADP, which has a signal-to-noise ratio of 17 for either the α or the β phosphate group (Supplementary Fig. 2*B*). Therefore, detecting ATP via 2DOGP using ^{1}H NMR signals significantly reduces the detection limit for ATP and shortens the data acquisition time.

ATP production using one-dimensional ^{1}H NMR spectroscopy. Highly sensitive one-dimensional ^{1}H NMR was used effectively to monitor 2DOGP production from 2DOG. The ^{1}H NMR spectra of 2DOG and 2DOGP were clearly different (Fig. 4*A*). In particular, the resonances of H6β, H4α, H4β, and H5β protons of 2DOGP are resolved from 2DOG peaks. Moreover, the H2α protons at ~1.7 ppm and H2β protons at ~1.5 ppm are partially resolved from each other (Fig. 4*A*). Because this region (1.4–1.8 ppm) of the ^{1}H NMR spectra is generally free from other overlapping peaks among the mitochondrial samples tested, we used H2α protons at ~1.7 ppm and H2β protons at ~1.5 ppm to monitor their peak intensity changes as affected by various ADP concentrations in control (Fig. 4*B*) and STZ-diabetic (Fig. 4*C*) mitochondrial incubates. Figure 4*B* and *C* clearly shows that under identical experimental conditions, the control mitochondria produced substantially more 2DOGP (or ATP) than the diabetic mitochondria.

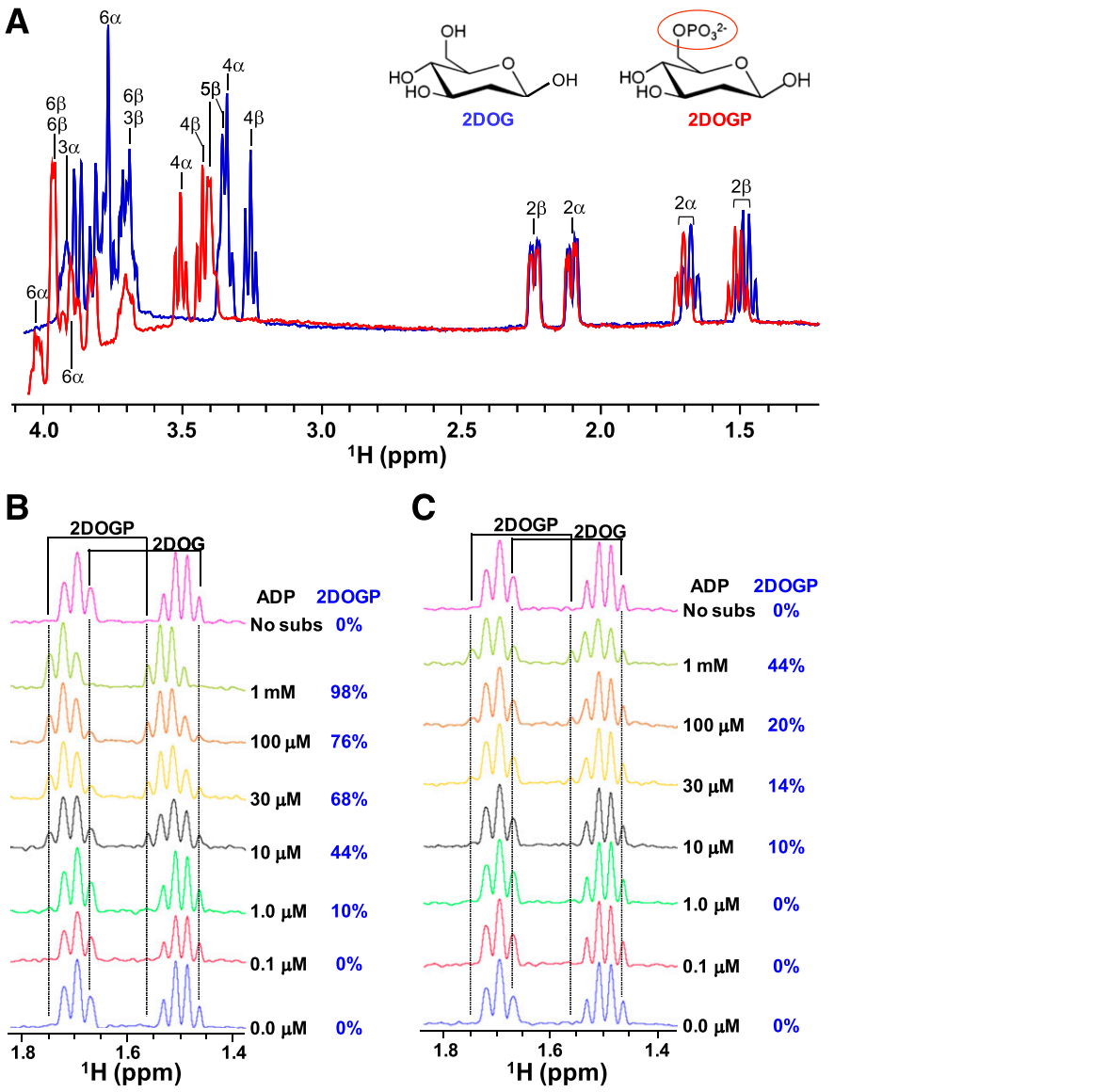

FIG. 4. Quantification of ATP production in control and diabetic mitochondria by one-dimensional ^{1}H NMR. *A*: Overlay of one-dimensional ^{1}H NMR spectra of 2DOG (blue) and 2DOGP (red). The resonance assignments are indicated. Regions of one-dimensional ^{1}H NMR spectra of 2DOG and 2DOGP of gastrocnemius mitochondrial samples isolated from a control (*B*) and diabetic (*C*) rat. Mitochondria (0.006 mg) were incubated in 60 μL of respiratory buffer with 5 mmol/L 2DOG, 5 units/mL hexokinase, and variable concentrations of ADP, and fueled with 5 mmol/L succinate plus 5 mmol/L glutamate plus 1 mmol/L malate for 20 min. Mitochondria were then precipitated and 40 μL supernatant was diluted into a final volume of 480 μL in NMR buffer. A total of 384 scans were collected for each sample. Quantification of the percent conversion of 2DOG into 2DOGP was performed by using the peak intensities of 2α and 2β protons of 2DOG and 2DOGP. ADP concentrations and the percent of 2DOGP converted from 2DOG are indicated to the right of the spectra. No subs = control with no added substrate or ADP.

ATP production using two-dimensional ^{1}H/^{13}C NMR spectroscopy. The two-dimensional ^{1}H/^{13}C heteronuclear multiple quantum coherence spectra of 2DOG and 2DOGP were assigned (Fig. 5*A*). The C6/H6 and C4/H4 cross-peaks of 2DOGP clearly were resolved from those of 2DOG. Using 2DOG with ^{13}C-labeling only at C6 position, i.e., [6-^{13}C] 2DOG, we can zoom-in to the C6 region (boxed in Fig. 5*A*) and collect high-resolution two-dimensional ^{1}H/^{13}C HSQC NMR spectra of control versus diabetic mitochondrial samples (Fig. 5*B*). Clearly, the cross-peaks derived from 2DOGP are well-resolved from those of 2DOG. Moreover, the cross-peaks of the α- and β-anomeric forms of those compounds are now well-resolved. Therefore, the amount of 2DOGP being converted from 2DOG can be reliably quantified by measuring the peak intensities in the contour plot or via the one-dimensional slices through the relevant cross-peaks (Fig. 5*B*). Because the C6/H6 cross-peak derived from the β-anomeric form of 2DOGP has the highest intensity, it is routinely chosen to quantify the amount of 2DOGP formed as a result of ATP production by mitochondria. Figure 5*B* clearly demonstrates that under identical experimental conditions, the diabetic mitochondrial sample produced much less 2DOGP or ATP than the control mitochondrial sample. This two-dimensional NMR method is sensitive, with a signal-to-noise ratio of 698 for the C6/H6 cross-peak of the β-anomeric form of 2DOGP (Supplementary Fig. 3) obtained by using a sample at the same concentration and with the same acquisition time as shown in Supplementary Fig. 2. Because of the narrow spectral width in the ^{13}C-dimension, it only took 4.5 min to acquire the high-resolution two-dimensional spectrum for the concentrated sample shown in Fig. 5*B*. For a typical

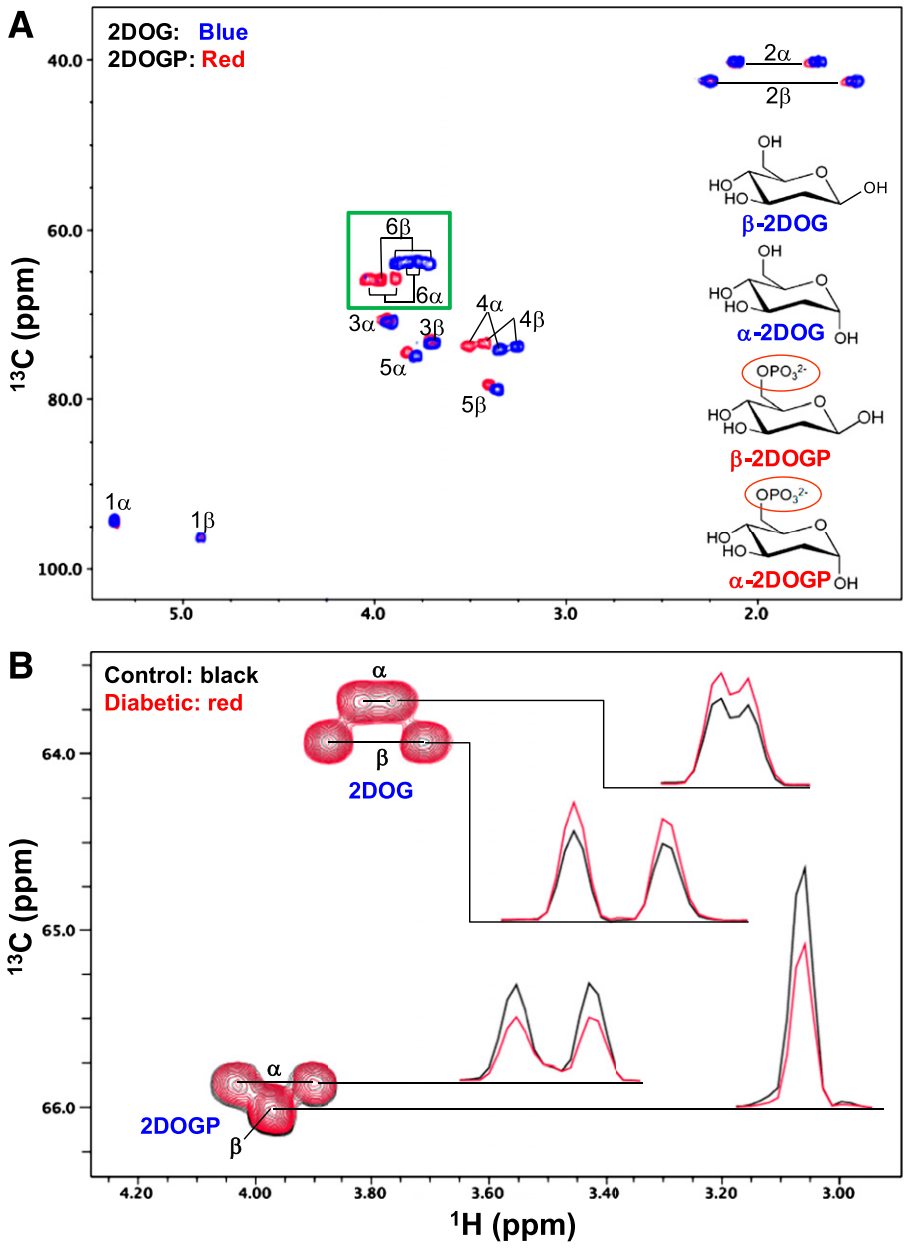

FIG. 5. Quantification of ATP production in control and diabetic mitochondria by two-dimensional ^{1}H/^{13}C NMR. *A*: Overlay of two-dimensional ^{1}H/^{13}C heteronuclear multiple quantum coherence spectra of unlabeled 2DOG (blue) and 2DOGP (red). The green box indicates the H6/C6 region of interest. The α- and β-anomeric structures of 2DOG and 2DOGP are included. The cross-peaks of the α- and β-anomeric forms are assigned. *B*: Overlay of two-dimensional ^{1}H/^{13}C HSQC spectra of the H6/C6 region of 2DOG and 2DOGP for samples that contain mitochondria from a control (black) rat and a diabetic (red) rat. Mitochondria (0.1 mg/mL) were incubated for 20 min in respiratory buffer containing 5.0 mmol/L [6-^{13}C]2DOG, 5 units/mL hexokinase, and 1 mmol/L ADP, and fueled with 5 mmol/L succinate, 5 mmol/L glutamate, and 1 mmol/L malate. Mitochondria were then precipitated by centrifugation and 50 μL D_2O was added to 450 μL supernatant for NMR studies. Each spectrum only took 4.5 min to acquire because the samples contained high concentrations of 2DOG and 2DOGP. The cross-peaks are labeled and one-dimensional slices through the cross-peaks are included.

mitochondrial NMR sample that contained ~0.42 mmol/L [6-^{13}C]2DOG initially, we acquired 15 complex t_1 increments with 16 scans per increment and a long recycle time of 4.4 s per scan, leading to a total acquisition time of 35 min (Supplementary Fig. 4). Most importantly, with the use of [6-^{13}C]2DOG, the acquired two-dimensional NMR spectra are clean, with no interference from background signals, even for samples that contain larger amounts of mitochondria or in the presence of different inhibitors used to assess mitochondrial function.

ATP detection limits. As shown in Supplementary Fig. 5*A*–*F*, we detected ATP production in mitochondrial samples at a concentration of 0.01 mg/mL in an incubation volume of 60 μL or a sample of 0.6 μg mitochondria. Conventional ^{31}P NMR was insensitive even at the highest mitochondrial concentration (Supplementary Fig. 5*G* and *H*).

Time effect after addition of oligomycin and effect of shaking during incubation. The time period between addition of oligomycin and completion of centrifugation to separate mitochondria (4 min) did not impact our results. In pilot experiments (Supplementary Fig. 6*A*), we removed mitochondria from the incubation mixture immediately (less than 30 s) after adding oligomycin by rapid filtration (versus centrifugation) and observed no difference in ATP

production. Mitochondria were not routinely shaken or stirred during incubation in the plate reader. However, it is possible to intermittently shake the wells within the plate reader between fluorescent reading cycles. Shaking in this way did not alter ATP production (Supplementary Fig. 6*B*).

ATP production rates on different substrate and inhibitor combinations. Our studies of diabetic and control mitochondria were performed using a combination of glutamate, malate, and succinate. However, as shown in Supplementary Fig. 7, our assay also can be used for different substrate conditions with the expected effects of the classic inhibitors, rotenone, oligomycin, and carbonyl cyanide p-[trifluoromethoxy]-phenyl-hydrazone.

ATP production rates in gastrocnemius mitochondria at clamped levels of ADP and potential. We measured ATP production by one-dimensional ^{1}H NMR as a function of added ADP for control, diabetic, and insulin-treated diabetic rats following protocol 1. As shown in Fig. 6*A*, for each amount of ADP added, diabetic mitochondria generated less ATP than controls. Mitochondria isolated from the insulin-treated diabetic rats produced amounts of ATP equivalent to controls. Plotting the same ATP data versus $\Delta\Psi$ (generated at each level of added ADP) again showed that the diabetic mitochondria produced less ATP compared with mitochondria of controls or from insulin-treated diabetic rats (Fig. 6*B*).

ROS production by gastrocnemius muscle of control and diabetic mitochondria. We examined the relationships between ROS production and inner membrane potential, as well as ROS production per unit ATP generated in gastrocnemius mitochondria of protocol 1 animals at various levels of clamped ADP (and, consequently, clamped, $\Delta\Psi$). The probe DHPA did not interfere with the ATP assay (Supplementary Fig. 8*A*), enabling concurrent assessment of ROS in the same 96-well plates. Both ATP and H_2O_2 concentrations increased in linear fashion during incubation (Supplementary Fig. 8). Respiration and $\Delta\Psi$ were assessed in parallel. Figure 7*A* depicts plateau levels of $\Delta\Psi$ as created by different concentrations of added ADP or ATP in STZ-DM, DM-INS, and control mitochondria. As expected, ROS production becomes very low at ADP concentrations high enough to drive mitochondria toward state 3 respiration (Fig. 7*B*). However, it is clear that ROS production by STZ-DM mitochondria begins to increase at a lower $\Delta\Psi$ threshold compared with control or DM-INS mitochondria. As shown in Fig. 7*C*, respiration, at any given $\Delta\Psi$, is reduced in mitochondria of STZ-DM rats compared with controls and DM-INS. As shown in Fig. 7D, the reduced $\Delta\Psi$ threshold effect for ROS is more evident when ROS production is viewed in relation to electron transport activity (proportional to respiration). Finally, ROS production per ATP generated is significantly higher in diabetic mitochondria (Fig. 7*E*).

ATP production rates in gastrocnemius mitochondria as a function of membrane potential independent of [ADP]. Although Fig. 6*B* depicts ATP production at different potential, these levels of $\Delta\Psi$ were achieved by varying [ADP]. To assess ATP production as a function of module 3 in Fig. 1, it is necessary to manipulate potential apart from a means that is, itself, operative in module 3. Therefore, we varied potential through titration with different substrate concentrations at the same ADP concentration (100 μmol/L). We incubated mitochondria in the presence of combined substrates using a constant ratio of 5:5:1 for succinate to glutamate to malate, with values for succinate and glutamate of 0.5, 1.0, 2.0, and 4.0 mmol/L and values for malate of 0.1, 0.2, 0.4, and 0.8 mmol/L.

These experiments were performed in rats treated according to protocol 2 (Fig. 2), and ATP production was assessed using two-dimensional ^{1}H/^{13}C HSQC NMR. As indicated in Fig. 8*A*, ATP production is linear with time for 30 min under the conditions of study. Therefore, ATP production rates were assessed over 30 min in all experiments. ATP production was decreased in both STZ-DM and DM-INS mitochondria compared with controls at the higher substrate concentrations (Fig. 8*B*).

At approximately the same time and on the same mitochondrial preparations, respiration and potential were measured in our respiratory chamber with sequential additions of substrates to achieve the desired concentrations. Respiration and potential increased with each increase of substrates and stabilized at plateau levels

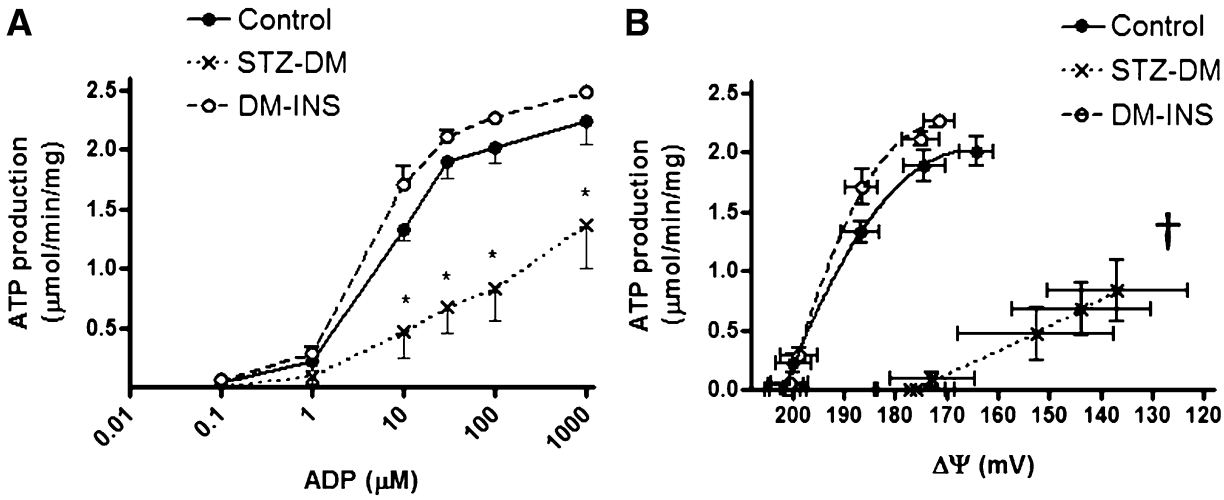

FIG. 6. Effect of STZ-DM and DM-INS on gastrocnemius muscle mitochondrial ATP production. *A*: ATP production rates as a function of ADP concentration for mitochondria isolated from control, STZ-DM, and DM-INS rats treated according to protocol 1 (Fig. 2; n = 4 per group). Mitochondria were incubated for 20 min and processed as described in the legend of Fig. 4. DHPA (20 μmol/L) was included in each well for simultaneous assessment of ROS (Fig. 7). *B*: ATP production rates for samples of *A* expressed as a function of $\Delta\Psi$. *P < 0.01 compared with control by two-way ANOVA; †P < 0.001 for difference in second-order polynomial curve fit models by F-test.

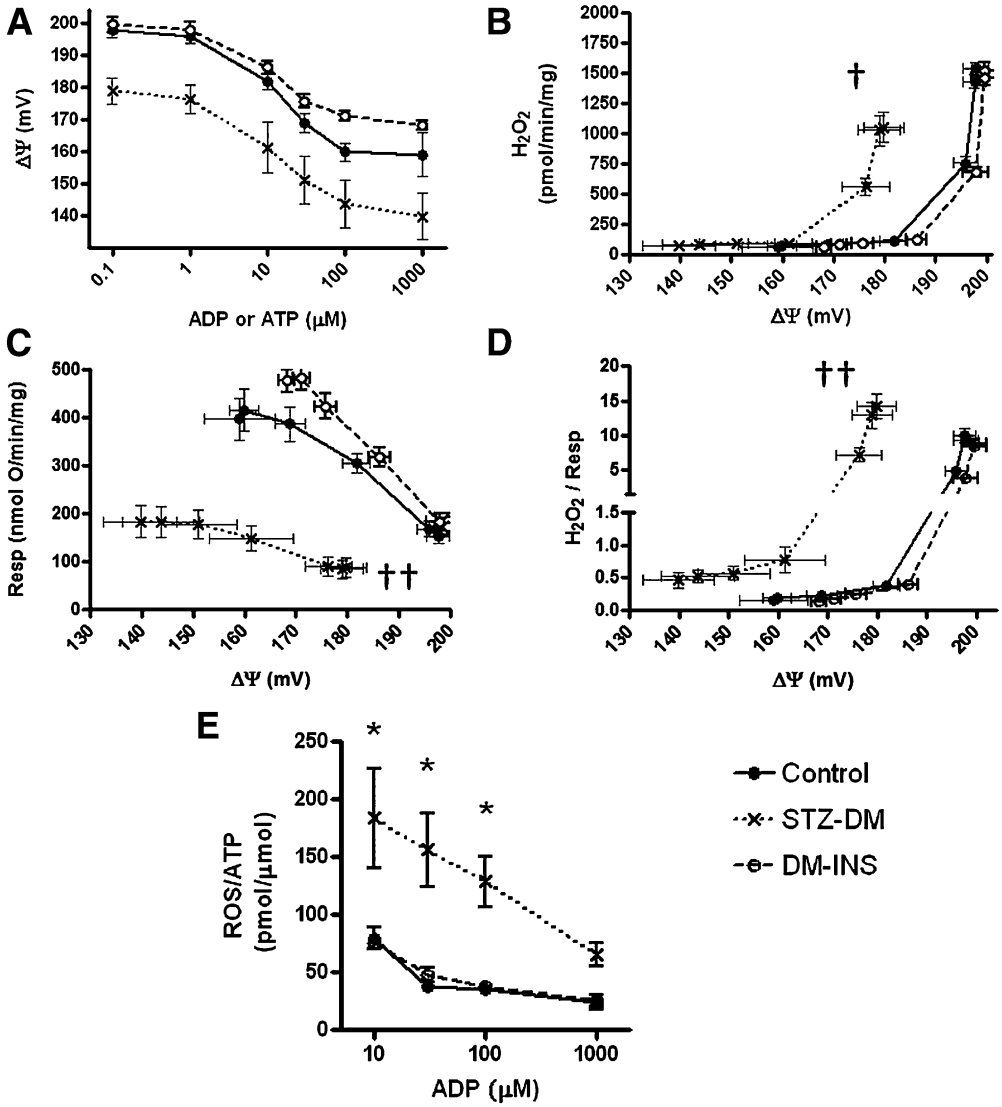

FIG. 7. Mitochondrial ROS production relative to ΔΨ in control, STZ-DM, or DM-INS rats treated according to protocol 1 (Fig. 2). Mitochondria were incubated for 20 min as described in the legend of Fig. 4. The data in *A–D* include the mitochondrial incubates from the four rats (per group) depicted in Fig. 6 plus additional mitochondrial incubates from additional rats wherein ATP was added rather than ADP (same concentrations). Essentially, the same data were obtained using either adenine nucleotide (as expected given the recycling effect), so the results were combined (total n = 8, 8, 7 for control, STZ-DM, and DM-INS, respectively). *A*: ΔΨ as a function of ADP or ATP concentration. *B*: Absolute H_2O_2 production as a function of ΔΨ. *C*: Respiration as a function of ΔΨ. *D*: H_2O_2 per oxygen consumed vs. ΔΨ. *E*: H_2O_2 produced per unit of ATP generated as a function of ADP added (n = 4 per group, all using ADP). Data of *E* do not include ADP concentrations <10 μmol/L because ATP formation is very low (Fig. 6) and H_2O_2 production is high, so that the denominator effect causes marked variability in the ratio. †P < 0.05 or ††P < 0.01 for difference in second-order polynomial curve fit models by F-test. *P < 0.01 compared with control by two-way ANOVA.

before the next addition, generating a range of potentials. Thus, we determined the relationship of ATP production to ΔΨ in control, STZ-DM, and DM-INS rats under conditions in which ATP production was dependent on potential in a manner reflecting module 3 of Fig. 1. The results (Fig. 8*C–E*) revealed that ATP production, as expected, increased with potential. However, the slope of that relationship was reduced in the STZ-DM and DM-INS mitochondria compared with controls (Fig. 8*F*), indicating a reduced capacity to utilize increments in potential to generate ATP.

DISCUSSION

We applied novel methodology to enable a more detailed evaluation of mitochondrial function as affected by insulin-deficient diabetes. There are several advantages to our ATP assay. First, the assay is performed under clamped ΔΨ, allowing assessment of ATP as a function of its direct driving force, ΔΨ. Second, our assay is sensitive enough to measure ATP production in small isolates of mitochondria. As indicated in Supplementary Figs. 2 and 3, the one-dimensional ^{1}H NMR method is 34-fold more sensitive and the two-dimensional $^{1}H/^{13}C$ HSQC NMR method is 41-fold more sensitive when compared with one-dimensional ^{31}P NMR for ATP detection. The high sensitivity of the two-dimensional NMR method is attributable to the fact that the chemical shifts of the two H6 protons of the β-anomeric form of 2DOGP are degenerate, resulting in detection of one single C6/H6 HSQC cross-peak with high intensity. Third, both the one-dimensional and two-dimensional NMR spectra are highly specific. In particular, the two-dimensional NMR method involves almost no interference from background signals. Fourth, there is good throughput

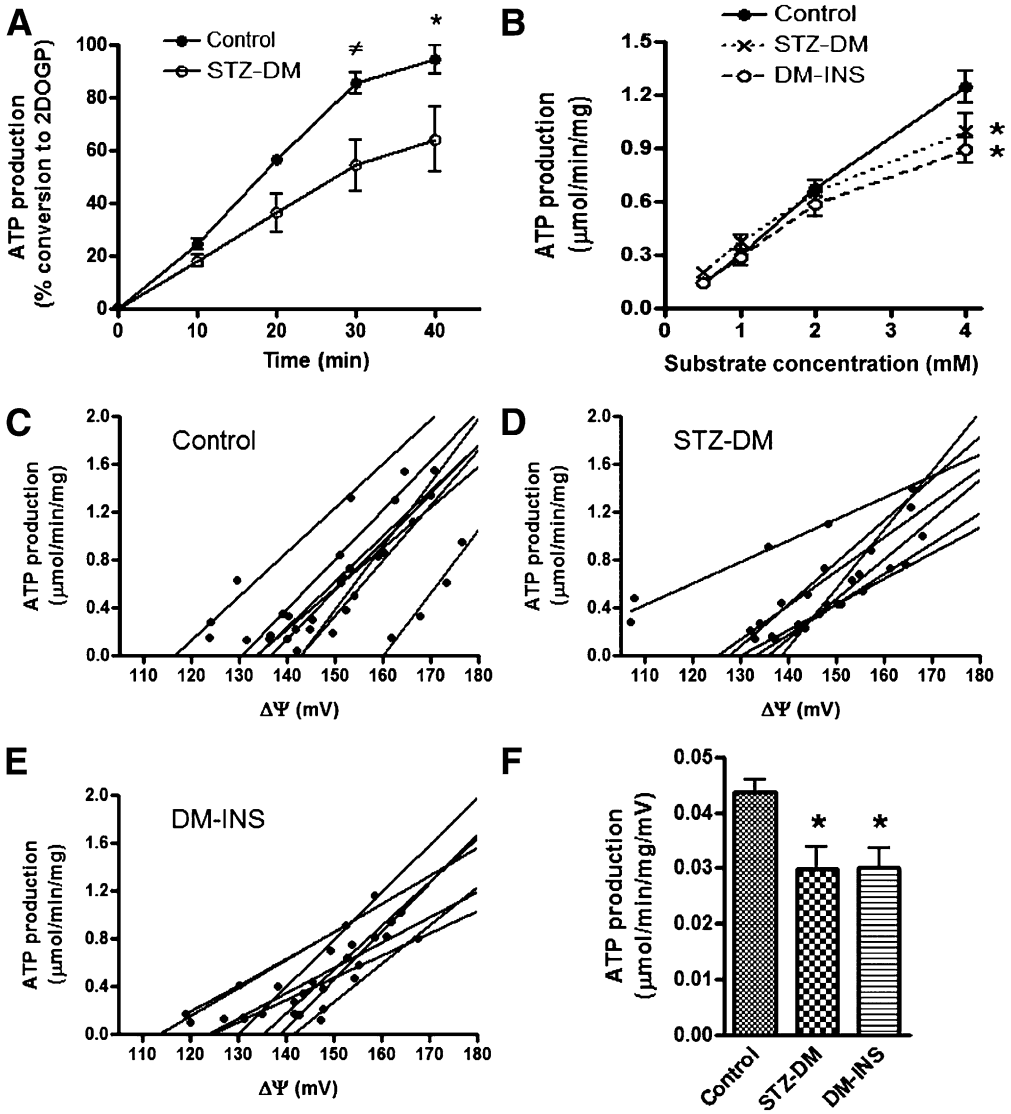

FIG. 8. Dependency of ATP production by gastrocnemius mitochondria on ΔΨ in control, STZ-DM, and DM-INS rats treated according to protocol 2 (Fig. 2). Membrane potential was modulated by incubating mitochondria in the presence of different substrate concentrations (combined succinate and glutamate each at 0.5, 1.0, 2.0, and 4.0 mmol/L, and malate at 0.1, 0.2. 0.4, and 0.8 mmol/L). *A*: Mitochondria were incubated in 96-well plates for 10, 20, 30, or 40 min in respiratory buffer containing 5 mmol/L [6-^{13}C]-2DOG and 5 units/mL HK in the presence of 4.0 mmol/L succinate, 4.0 mmol/L glutamate, and 0.8 mmol/L malate (n = 4 per group; *P < 0.05 or ≠P < 0.01 by two-way ANOVA compared with control). Similar linear, although lower, rates were observed for the lower substrate concentrations (not shown). Because ATP production was linear over the first 30 min, further studies (subsequent panels) were performed in mitochondria incubated for 30 min. *B*: ATP production as a function of substrate concentrations. The x-axis indicates only the concentrations of succinate and glutamate, although malate was included at 20% of the indicated values (n = 8, 7, and 7 for control, STZ-DM, and DM-INS mitochondria, respectively). *P < 0.01 compared with control by two-way ANOVA. *C–E*: In parallel experiments on the same mitochondrial preparations, mitochondria were incubated in our respiratory chamber at progressively increasing substrate concentrations (those used in the wells for ATP determination) to obtain values for ΔΨ. Data depict the relationship of ATP production to ΔΨ in control, STZ-DM, and DM-INS rats. Lines represent linear regression for each mitochondrial incubation. All regression analyses were significant (P < 0.05), with r^2 > 0.9. *F*: Slopes (mean ± SE) for the regressions in *C–E*. *P < 0.05 compared with control by one-way ANOVA and Tukey posttest.

because we can add mitochondria to multiple wells of a 96-well plate, incubate, spin-off the mitochondria, and save the samples that can be directly used for NMR analysis. Fifth, a powerful aspect of this technique is that we can assess mitochondrial ROS along with ATP formation rates simultaneously because the ROS probe (DHPA) does not interfere with the NMR signals of interest in either one-dimensional or two-dimensional NMR spectra. Moreover, DHPA does not interfere with ATP production (Supplementary Fig. 8*A*). It also may be possible to use TMRM or other probes to simultaneously assess potential, although preliminary experiments indicate that higher TMRM concentration may mildly reduce ATP production.

The methods described here have clear advantages over existing methods for ATP assay. Fluorescent and bioluminescent measurements are sensitive, but not specific, and are prone to background interference or variations in light emission (23). Phosphorous NMR is not sensitive enough and requires long acquisition times unless large numbers of mitochondria are used. High-performance liquid chromatography has been used when precise data are needed, but it is cumbersome. ATP:O ratios often are reported as indicative of ATP production because of these difficulties. However, this does not measure ATP and the ratio can be altered by any condition that affects uncoupling, ATP synthase, and respiration itself. Even compared with

high-resolution respirometry with luminescent detection of ATP, our method has clear advantages. It is more specific, can be performed with far more throughput involving 96-well plates as compared with dual chambers, can measure ATP at clamped ADP and potential, and can simultaneously measure other fluorescent signals. Of course, the 2DOG technique could be used to clamp potential in the high-resolution respirometer. However, if this were performed, then one could not use reagents such as luciferase (24) or magnesium green (25) to assess ATP production because the 2DOG/hexokinase reaction would compete for ATP.

The energy clamp/ATP assay allowed us to perform novel studies, which was not previously possible. We show that gastrocnemius muscle mitochondria isolated from diabetic rats generate less ATP at any given clamped level of ADP availability (Fig. 6). Thus, the reduction in ATP production occurs throughout progression from state 4 to state 3 respiration. In addition, we investigated the capacity of ATP production to directly utilize $\Delta\Psi$ (Fig. 8*C–F*). Although respiration and proton leaks (modules 1 and 2) determine membrane potential, according to the chemiosmotic hypothesis, it is only potential itself that drives ATP synthase (1). So, the different dynamic relationship of ATP production relative to potential (manipulated independent of module 3) in the diabetic mitochondria (Fig. 8*F*) implies an inability of ATP synthase to effectively utilize potential for ATP synthesis. This is important because it implicates a functional defect within module 3 of oxidative phosphorylation.

With regard to ROS, we used the 2DOG energy clamp to provide novel information about the relationship of ROS production to $\Delta\Psi$ (Fig. 7). We and others recently reported (26,27) that absolute ROS production from muscle and heart mitochondria is not increased, or is decreased, in mitochondria of insulin-deficient diabetic rodents. In further work (5), we showed that ROS production expressed per unit of electron transport is actually increased in muscle and heart mitochondria. Here, we used the 2DOG clamp technology to provide new data indicating a $\Delta\Psi$ threshold effect (Fig. 7*B* and *D*) for ROS production, which is lower in diabetic mitochondria (move ROS at lower potential). In addition, we provide novel data indicating that, for any given level of added ADP, ROS per unit of ATP generated is increased (Fig. 7*E*) in diabetic mitochondria. In other words, the ROS "cost" of ATP production is markedly increased for mitochondria of STZ-diabetic rodents. With respect to this, we point out an important advantage of expressing ROS production per unit of respiration or per unit of ATP production. These metrics are independent of mitochondrial mass, simply because the units of mass in the numerators and denominators cancel. Finally, we show that the defective ATP production by diabetic mitochondria is reversible, at least with sufficient duration of treatment.

Why should insulin deficiency and insulin treatment impact ATP production? Decreased expression of several genes regulating ATP synthase as well as other genes involved in modules 1 and 3 of Fig. 1 have been reported in skeletal muscle and heart of insulin-deficient rodents and humans (28–31). Our studies, for the first time, implicate a functional defect at the level of module 3 contributing to reduced ATP production. This could occur because of a diabetes-induced decrease in expression of any component of ATP synthase, impaired ADP delivery to the mitochondrial matrix, or a perturbation in any factor regulating the activity of the ATP synthase complex. In fact, as recently reviewed (32), a myriad of proteins, various ions, and membrane structure or folding all could alter ATP synthase.

Aside from defects in oxidative phosphorylation at the level of module 3, decreased respiration (module 1) clearly contributes by decreasing $\Delta\Psi$, but not to the capacity to utilize $\Delta\Psi$. Uncoupling (module 2) also could affect ATP production by reducing $\Delta\Psi$, but, again, not to the capacity to utilize $\Delta\Psi$. However, based on our past studies of insulin-deficient gastrocnemius mitochondria, uncoupling does not likely play a role in reducing mitochondrial ATP production, because proton conductance was, if anything, decreased (8). This is also consistent with a reported lack of change in uncoupling in heart mitochondria of insulin-deficient mice (27).

Karakelides et al. (28) assessed muscle mitochondrial ATP production by bioluminescence in units of μmol/min/g of tissue. ATP production was reduced in biopsy samples of subjects with type 1 diabetes after transient withdrawal of insulin therapy. Our results agree and extend observations to the direct utilization of $\Delta\Psi$ and to simultaneous measurement of ROS with ATP at clamped potential. Our results agree with the data of Kacerovsky et al. (33), who used in vivo saturation transfer to assess the exchange between phosphate and ATP by ^{31}P NMR. These investigators reported that insulin-stimulated unidirectional flux through ATP synthesis was reduced in eight type 1 diabetic subjects.

In protocol 2, we included short-duration insulin-treated rats to see if this would restore ATP production, as occurred after longer-duration insulin therapy in protocol 1. As shown (Fig. 8*B*), this was not the case. We can only speculate as to possible reasons. Multiple cellular pathways may require time to adjust as muscle converts from a catabolic (insulin-deficient) to an anabolic recovery state. Moreover, insulin strongly impacts fatty acid flux. Conceivably, this could alter mitochondrial lipid composition in a time-dependent manner, which might then alter the activity of ATP synthase or other mitochondrial membrane proteins.

We acknowledge some differences between protocols 1 and 2, but we doubt that these explain the lack of recovery with the shorter duration of insulin. Substrate concentrations used in the ATP production studies of protocol 1 (Fig. 6) and protocol 2 (Fig. 8*B*) were not exactly the same but were similar (5 mmol/L glutamate and succinate and 1 mmol/L malate in protocol 1 compared with maximal concentrations of 4, 4, and 0.8 mmol/L, respectively, in protocol 2), and, within each protocol, substrate concentrations were identical for all treatment groups. Also, we used one-dimensional NMR for protocol 1 but elected to proceed to the two-dimensional technique for the protocol 2 studies. However, both the one-dimensional and two-dimensional methods generated very clean signals with excellent sensitivity. The time period of diabetes (after STZ treatment until euthanization) was somewhat shorter in protocol 2 and the insulin dose was larger. However, we would expect those factors to favor rather than hinder the recovery of ATP production.

A limitation is that we did not come close to normalizing the glucose in our insulin-treated rats. However, that is difficult or impossible in STZ-DM, and we did observe substantial body weight recovery given adequate time. Another limitation is simply that isolated mitochondria, as opposed to in vivo techniques such as phosphocreatine and ATP resynthesis and ATP saturation transfer (34), do not consider the external environment. Conversely, studies of isolated mitochondria remain the only way to assess intrinsic mitochondrial properties altered by preexisting physiologic states. Moreover, our ATP methods have an advantage in that clamped ADP and

potential are more physiologic than what occurs by conventional mitochondrial methods wherein ADP concentrations continuously decrease and $\Delta\Psi$ continuously increases after addition of ADP.

In summary, we report several novel findings. We show, for the first time, that the mechanism by which ATP production is reduced in mitochondria of insulin-deficient diabetic rats involves, at least in part, a functional defect in module 3 of oxidative phosphorylation. Defective ATP production by diabetic mitochondria is evident across a range from state 3 to 4 respiration. ROS production (absolute and per unit of electron transport) begins to increase in muscle mitochondria of insulin-deficient rats at a lower $\Delta\Psi$ threshold. The ROS "cost" of ATP production is greater in mitochondria from insulin-deficient rats. Defective ATP production is reversible in diabetic mitochondria by insulin treatment but, subject to limitations of our protocols, appears dependent on adequate duration of therapy. We describe a novel method for assessing ATP production that enables these studies and possesses advantages applicable to a myriad of future projects.

ACKNOWLEDGMENTS

This work was supported by Veterans Affairs Medical Research Funds, the National Institutes of Health (5R01HL073166), and by the Iowa Affiliate Fraternal Order of Eagles.

No potential conflicts of interest relevant to this article were reported.

L.Y. wrote the manuscript, participated in design, and conducted experiments. B.D.F. participated in design, conducted experiments, and reviewed and edited the manuscript. J.A.H. conducted experiments. W.I.S. wrote the manuscript, participated in design, and conducted experiments. W.I.S. is the guarantor of this work and, as such, had full access to all the data in the study and takes responsibility for the integrity of the data and the accuracy of the data analysis.

Parts of this study were presented at the 72nd Scientific Sessions of the American Diabetes Association, Philadelphia, Pennsylvania, 8–12 June 2012.

REFERENCES

1. Mitchell P. Coupling of phosphorylation to electron and hydrogen transfer by a chemi-osmotic type of mechanism. Nature 1961;191:144–148
2. Fillingame RH, Dmitriev OY. Structural model of the transmembrane Fo rotary sector of H+-transporting ATP synthase derived by solution NMR and intersubunit cross-linking in situ. Biochim Biophys Acta 2002;1565:232–245
3. von Ballmoos C, Cook GM, Dimroth P. Unique rotary ATP synthase and its biological diversity. Annu Rev Biophys 2008;37:43–64
4. Brand MD, Nicholls DG. Assessing mitochondrial dysfunction in cells. Biochem J 2011;435:297–312
5. Herlein JA, Fink BD, Henry DM, Yorek MA, Teesch LM, Sivitz WI. Mitochondrial superoxide and coenzyme Q in insulin-deficient rats: increased electron leak. Am J Physiol Regul Integr Comp Physiol 2011;301:R1616–R1624
6. Takaki M, Nakahara H, Kawatani Y, Utsumi K, Suga H. No suppression of respiratory function of mitochondrial isolated from the hearts of anesthetized rats with high-dose pentobarbital sodium. Jpn J Physiol 1997;47:87–92
7. Fink BD, Reszka KJ, Herlein JA, Mathahs MM, Sivitz WI. Respiratory uncoupling by UCP1 and UCP2 and superoxide generation in endothelial cell mitochondria. Am J Physiol Endocrinol Metab 2005;288:E71–E79
8. Herlein JA, Fink BD, O'Malley Y, Sivitz WI. Superoxide and respiratory coupling in mitochondria of insulin-deficient diabetic rats. Endocrinology 2009;150:46–55
9. Hong Y, Fink BD, Dillon JS, Sivitz WI. Effects of adenoviral overexpression of uncoupling protein-2 and -3 on mitochondrial respiration in insulinoma cells. Endocrinology 2001;142:249–256
10. Wojtczak L, Zaluska H, Wroniszewska A, Wojtczak AB. Assay for the intactness of the outer membrane in isolated mitochondria. Acta Biochim Pol 1972;19:227–234
11. Fink BD, Herlein JA, Almind K, Cinti S, Kahn CR, Sivitz WI. Mitochondrial proton leak in obesity-resistant and obesity-prone mice. Am J Physiol Regul Integr Comp Physiol 2007;293:R1773–R1780
12. O'Malley Y, Fink BD, Ross NC, Prisinzano TE, Sivitz WI. Reactive oxygen and targeted antioxidant administration in endothelial cell mitochondria. J Biol Chem 2006;281:39766–39775
13. Rhee SG, Chang TS, Jeong W, Kang D. Methods for detection and measurement of hydrogen peroxide inside and outside of cells. Mol Cells 2010; 29:539–549
14. da-Silva WS, Gómez-Puyou A, de Gómez-Puyou MT, et al. Mitochondrial bound hexokinase activity as a preventive antioxidant defense: steady-state ADP formation as a regulatory mechanism of membrane potential and reactive oxygen species generation in mitochondria. J Biol Chem 2004; 279:39846–39855
15. Rance M, Sørensen OW, Bodenhausen G, Wagner G, Ernst RR, Wüthrich K. Improved spectral resolution in cosy ^{1}H NMR spectra of proteins via double quantum filtering. Biochem Biophys Res Commun 1983;117:479–485
16. Braunschweiler L, Ernst RR. Coherence transfer by isotropic mixing: Application to proton correlation spectroscopy. J Magn Reson 1983;53:521–528
17. Bax A, Davis DG. MLEV-17-based two-dimensional homonuclear magnetization transfer spectroscopy. J Magn Reson 1985;65:355–360
18. Nyberg NT, Sørensen OW. Multiplicity-edited broadband HMBC NMR spectra. Magn Reson Chem 2006;44:451–454
19. Palmer AG, Cavanagh J, Wright PE, Rance M. Sensitivity improvement in proton-detected two-dimensional heteronuclear correlation NMR spectroscopy. J Magn Reson 1991;93:151–170
20. Olsson U, Lycknert K, Stenutz R, Weintraub A, Widmalm G. Structural analysis of the O-antigen polysaccharide from Escherichia coli O152. Carbohydr Res 2005;340:167–171
21. Delaglio F, Grzesiek S, Vuister GW, Zhu G, Pfeifer J, Bax A. NMRPipe: a multidimensional spectral processing system based on UNIX pipes. J Biomol NMR 1995;6:277–293
22. Johnson BA, Blevins RA. NMR View: A computer program for the visualization and analysis of NMR data. J Biomol NMR 1994;4:603–614
23. Manfredi G, Spinazzola A, Checcarelli N, Naini A. Assay of mitochondrial ATP synthesis in animal cells. Methods Cell Biol 2001;65:133–145
24. Lundin A. Use of firefly luciferase in ATP-related assays of biomass, enzymes, and metabolites. Methods Enzymol 2000;305:346–370
25. Chinopoulos C, Vajda S, Csanády L, Mándi M, Mathe K, Adam-Vizi V. A novel kinetic assay of mitochondrial ATP-ADP exchange rate mediated by the ANT. Biophys J 2009;96:2490–2504
26. Herlein JA, Fink BD, Sivitz WI. Superoxide production by mitochondria of insulin-sensitive tissues: mechanistic differences and effect of early diabetes. Metabolism 2010;59:247–257
27. Bugger H, Boudina S, Hu XX, et al. Type 1 diabetic akita mouse hearts are insulin sensitive but manifest structurally abnormal mitochondria that remain coupled despite increased uncoupling protein 3. Diabetes 2008;57: 2924–2932
28. Karakelides H, Asmann YW, Bigelow ML, et al. Effect of insulin deprivation on muscle mitochondrial ATP production and gene transcript levels in type 1 diabetic subjects. Diabetes 2007;56:2683–2689
29. Basu R, Oudit GY, Wang X, et al. Type 1 diabetic cardiomyopathy in the Akita (Ins2WT/C96Y) mouse model is characterized by lipotoxicity and diastolic dysfunction with preserved systolic function. Am J Physiol Heart Circ Physiol 2009;297:H2096–H2108
30. Chowdhury SK, Zherebitskaya E, Smith DR, et al. Mitochondrial respiratory chain dysfunction in dorsal root ganglia of streptozotocin-induced diabetic rats and its correction by insulin treatment. Diabetes 2010;59: 1082–1091
31. Johnson DT, Harris RA, French S, Aponte A, Balaban RS. Proteomic changes associated with diabetes in the BB-DP rat. Am J Physiol Endocrinol Metab 2009;296:E422–E432
32. Johnson JA, Ogbi M. Targeting the F1Fo ATP Synthase: modulation of the body's powerhouse and its implications for human disease. Curr Med Chem 2011;18:4684–4714
33. Kacerovsky M, Brehm A, Chmelik M, et al. Impaired insulin stimulation of muscular ATP production in patients with type 1 diabetes. J Intern Med 2011;269:189–199
34. Szendroedi J, Phielix E, Roden M. The role of mitochondria in insulin resistance and type 2 diabetes mellitus. Nat Rev Endocrinol 2011;8:92–103